Bulgarian Chemical Communications, Volume 52, Issue 2 (pp. 259 - 271) 2020 DOI: 10.34049/bcc.52.2.5168

Stability analysis and multiple solutions of a hydromagnetic dissipative flow over a stretching/shrinking sheet

M. R. Mishra[1], S. M. Hussain[2*], O. D. Makinde[3], G. S. Seth[4]

[1]*Department of Mathematics, OP Jindal University, Raigarh, 496109, India*
[1,2]*Department of Mathematics, Faculty of Science, Islamic University of Madinah, 42351, Saudi Arabia*
[3]*Faculty of Military Science, Stellenbosch University, Private Bag X2, Saldanha, 7395, South Africa*
[4]*Department of Applied Mathematics, Indian Institute of Technology (ISM), Dhanbad, 826004, India*

Received: June 18, 2019; Revised: February 18, 2020

The steady hydromagnetic two-dimensional flow of a viscous, incompressible, optically thick radiative and electrically conducting fluid past a permeable stretching/shrinking sheet is studied. The effects of heat absorption, chemical reaction, viscous and Joule dissipations are taken into consideration. The governing mathematical equations comprising the partial differential equations are changed to the form of nonlinear ordinary differential equations by making use of the suitable similarity variables. Further, fourth order Runge-Kutta scheme along with a shooting technique is implemented to analyze the numerical solution. Moreover, the consequence of relatable physical parameters on the fluid velocity, temperature distribution and fluid concentration are quantified through different graphs whereas, from engineering viewpoint, the numerical findings of wall velocity gradient, Sherwood numbers and wall temperature gradient are provided in tabular form. Our results reveal that the stretching/shrinking parameter range is widened due to magnetic field and suction for which there is a solution. Meanwhile, the presence of dual solutions is observed in the range of prevailing parameters. The results obtained in the present study are compared and verified with the existing numerical results.

Keywords: Stability analysis; Dual solution; Viscous dissipation; Joule dissipation.

NOMENCLATURE

B_0	uniform magnetic field (T)	M	magnetic parameter ($\sigma B_0^{\,2} / a\rho$)
C_p	specific heat at constant pressure ($J/(kg\ K)$)	Pr	Prandtl number (υ / α)
D_B	mass diffusivity (m^2/s)	Q	heat absorption parameter ($Q_0 / a\,\rho C_p$)
Ec	Eckert number ($\bar{u}_w^{\,2} / C_p(T'_w - T'_\infty)$)	Q_0	heat absorption coefficient (W/(m^{2}K))
K	chemical reaction parameter (k_0 / a)	q_r	radiative heat flux ($W\ m^{-2}$)
k	thermal conductivity ($W\ m^{-1}$)	R	radiation parameter ($4\sigma^* T'^3_\infty / k\,k^*$)
k^*	mean absorption coefficient (cm^{-1})	S	suction/injection parameter ($-v_0 / \sqrt{a\upsilon}$)
k_0	constant rate of chemical reaction	Sc	Schmidt number (υ / D_B)
$\bar{T}$	fluid temperature (°K)	$\bar{v}$	velocity along y axis ($m\ s^{-1}$)
$\bar{u}$	velocity along x axis ($m\ s^{-1}$)		

GREEK SYMBOLS

α	fluid thermal diffusivity (m^2/s)	σ^*	Stefan Boltzmann constant ($W / m^2 K^4$)
$\bar{\beta}$	species concentration ($kg\ m^{-3}$)	σ	fluid electrical conductivity ($s^3\ A^2\ m^{-3} kg^{-1}$)
ϕ	dimensionless species concentration	μ	fluid dynamic viscosity ($kg\ m^{-1}\ s^{-1}$)
θ	dimensionless fluid temperature	υ	fluid kinematic viscosity (m^2/s)
ρ	density of fluid ($kg\ m^{-3}$)		

* To whom all correspondence should be sent:
E-mail: hussain.modassir@yahoo.com

SIGNIFICANCE STATEMENT

Analysis of a boundary layer hydromagnetic flow of a dissipative fluid over a stretching/shrinking sheet is noteworthy owing to its enormous significance in industry which includes electrical power generation, plastic substances manufacturing, solar power technology, extrusion of polymers, metallurgical process, etc. Influence of various physical parameters like magnetic field, stretching/shrinking, heat absorption, suction/ injection, thermal radiation, chemical reaction, etc. is quantified. Additionally, flow stability analysis is executed to analyze the physically reliable and stable solutions of the problem. Finally, validation of the numerical results is done in the limiting conditions with the previously published research paper of Yasin *et al*. [37].

INTRODUCTION

Substantial attention has been paid to the study of a hydrodynamic fluid flow over the past decades because of its enormous relevance, for instance, in heat storage systems, geophysics, oil recovery techniques, chemical processing equipment, thermal insulations, cosmic fluid dynamics, etc. Moreover, the imposition of exerted magnetic field onto the flow regime driven by non-permeable and permeable stretching sheets has engrossed the curiosity of researchers due to its significance in industry and public enterprise. The pioneering research on the magnetohydrodynamic fluid flow due to plane surface's deformation was executed by Pavlov [1]. Moreover, Chakrabarti and Gupta [2] explored this investigation considering temperature distribution. Al-Odat *et al*. [3] discussed the influence of exerted magnetic field on a boundary layer fluid flow permeated by a stretched sheet. Also, the hydromagnetic problems driven by a stretched sheet have been investigated in [4-7], etc.

Heat generation/absorption models of a fluid flow driven by a permeable stretched sheet have been investigated by many authors because of its numerous industrial applications, *viz*. hot rolling, chemical reaction that discharges heat, endothermic reactions, heat exchange from nuclear fuel wastage, glass fiber production, paper production, etc. Following this, Elbashbeshy [8] numerically analyzed the solution of a quiescent fluid flow over an exponentially stretched sheet amid the significance of heat source/sink. This study illustrates that the suction can be employed to cool down the moving continuous surface. Further, this problem was extended by Elbashbeshy and Bazid [9] considering an unsteady state condition. Subsequently, Eldahab and Aziz [10] considered the suction/blowing influence on a magnetohydrodynamic flow considering heat generation and absorption over the obliquely aligned stretched surface. Makinde *et al*. [11, 12] investigated the flow of a mixed convective magnetohydrodynamic nanofluid along a permeable stretched sheet.

The vital characteristics of thermal radiation for surface heat transfer cannot be ignored while considering industrial processes like electrical power generation, designing of furnace, production of glass, missiles devices, solar power technology, etc., wherein high temperature occurs. At the present industrial scenario, due to decrease of conventional energy resources, the attention is focused on sustainable and renewable energy sources. The solar energy is the main fountain of renewable energy and thermal radiation has a noteworthy role in transforming the solar energy to the appropriate form for various applications in industry. Owing to this reason, many authors [13-17], etc. have illustrated the significance of thermal radiation on the laminar fluid flow over a plate/stretching sheet.

In the above studies, the viscous dissipation effect has been ignored as the same is supposed to be low but its relevance in food processing, instrumentations, lubrications, polymer manufacturing, etc., is considered as very significant as it enhances the characteristics of temperature distribution which induce the heat transfer rate. Some important studies dealing with the viscous dissipative flow problem induced by stretched sheet are reported [18-21]. Further, Joule dissipation behaves like a volumetric heat source in magnetohydrodynamic fluid flows and the collective influence of viscous and Joule dissipations is imperative in context of the heat-treated materials. Following this, Anjali and Ganga [22], Pal [23], Seth and Singh [24] and Seth *et al.* [25, 26] modeled their problem considering the impacts of Joule and viscous dissipations. Seth *et al*. [27] explored the Joule dissipation effects on the flow of a magnetohydrodynamic (MHD) thin film Casson fluid over a flat stretched sheet.

The relevance of a chemical reaction on a hydromagnetic fluid flow has been a matter of excessive attention in the past few decades because of its large scientific and technological impacts like polymer and ceramics production, manufacturing of insulated cables and glassware, chemical processing of materials and many more. Some relevant studies reporting the effects of a chemical reaction are presented in [28-36]. Moreover, Yasin *et al*. [37] studied two-dimensional steady hydromagnetic flows driven by a permeable stretched or shrinking

sheet, taking into account heat absorption and thermal radiation.

The present paper has the objective to unfold the combined impacts of Joule and viscous dissipations on a two-dimensional MHD fluid, as well as the mass transfer of a heat absorbing, incompressible, thick radiative, electrically conducting viscous fluid permeated by a stretching/shrinking sheet in the presence of a homogeneous chemical reaction. Numerical solutions of the governing mathematical equations are obtained employing a 4th order Runge-Kutta scheme along with a shooting technique. Additionally, flow stability analysis is executed to examine the physically reliable and stable solutions of the problem. Finally, validation of the numerical results is done in the limiting conditions with a previously published research paper. The meticulous review of research papers reported in the literature revealed that none of the authors has earlier attempted this problem although the thoughts and methodology explained in this paper can be anticipated to lead to enormously prolific connections across the disciplines.

MATHEMATICAL ANALYSIS

Mathematical problem formulation

We consider the steady 2-dimensional dissipative hydromagnetic flow of a heat absorbing, incompressible, optically thick radiative, electrically conducting, viscous fluid, as well as mass transfer fluid driven by a stretched or shrinking sheet. The fluid is induced over the stretched or shrunk sheet owing to the velocity $\lambda\bar{u}_w(x)$ where $\lambda >$ or < 0 is considered for a stretched or a shrunk sheet. The transverse magnetic field B_0 is exerted along y direction (Fig. 1). For considering this fluid flow model, we have taken the x-axis along the stretched sheet surface whilst y-axis is normal to it, the flow being limited to $y > 0$. Further, the mass flux velocity of the stretching sheet is presumed as v_0 where $v_0 < 0$ and $v_0 > 0$ are, considered for suction and injection, respectively, as the surface is considered to be permeable. At a stretched/shrunk sheet surface, the temperature $\bar{T}_w$ and concentration $\bar{\beta}_w$ are supposed to be constant whilst ambient fluid is considered as $\bar{T}_\infty$ and $\bar{\beta}_\infty$. Moreover, a first-order homogeneous chemical reaction k_0 having constant rate is supposed to take place among the fluid and the diffusive species.

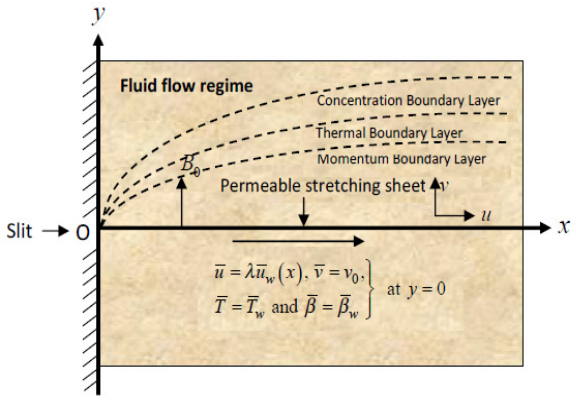

Figure 1. Physical model of the problem

The mathematical model for the fluid flow is represented as:

$$\frac{\partial\bar{u}}{\partial x} + \frac{\partial\bar{v}}{\partial y} = 0, \tag{1}$$

$$\bar{u}\frac{\partial\bar{u}}{\partial x} + \bar{v}\frac{\partial\bar{u}}{\partial y} = \upsilon\frac{\partial^2\bar{u}}{\partial y^2} - \frac{\sigma B_0{}^2}{\rho}\bar{u}, \tag{2}$$

$$\bar{u}\frac{\partial\bar{T}}{\partial x} + \bar{v}\frac{\partial\bar{T}}{\partial y} = \alpha\frac{\partial^2\bar{T}}{\partial y^2} + \frac{\upsilon}{C_p}\left(\frac{\partial\bar{u}}{\partial y}\right)^2 - \frac{1}{\rho C_p}\frac{\partial q_r}{\partial y} - \frac{Q_0}{\rho C_p}\left(\bar{T} - \bar{T}_\infty\right) + \frac{\sigma}{\rho C_p}B_0{}^2\bar{u}^2, \tag{3}$$

$$\bar{u}\frac{\partial\bar{\beta}}{\partial x} + \bar{v}\frac{\partial\bar{\beta}}{\partial y} = D_B\frac{\partial^2\bar{\beta}}{\partial y^2} - k_0\left(\bar{\beta} - \bar{\beta}_\infty\right). \tag{4}$$

The associated boundary conditions are:

$$\left.\begin{aligned} &\bar{u} = \lambda\bar{u}_w(x),\ \bar{v} = v_0,\ \bar{T} = \bar{T}_w,\ \bar{\beta} = \bar{\beta}_w \text{ when } y = 0, \\ &\bar{u} \to 0,\ \bar{\beta} \to \bar{\beta}_\infty \text{ and } \bar{T} \to \bar{T}_\infty \quad \text{for } y \to \infty, \end{aligned}\right\} \tag{5}$$

where $\bar{u}_w(x) = a\,x$ such that the constant $a > 0$.

The Rosseland approximation [38] for an optically thick radiative fluid is used to transform the radiative heat flux q_r as:

$$q_r = -\frac{4\sigma^*}{3k^*}\frac{\partial \overline{T}^4}{\partial y}. \tag{6}$$

Moreover, $\overline{T}^4$ is linearized by means of the Taylor's series expansion about $\overline{T}_\infty$ (free stream temperature) and then higher order terms are neglected. The linearized form is given by:

$$\overline{T}^4 \cong -3\overline{T}_\infty^4 + 4\overline{T}_\infty^3 \overline{T}\,. \tag{7}$$

Eqs. (6) and (7) transform the energy Eq. (3) in the following form:

$$\overline{u}\frac{\partial \overline{T}}{\partial x} + \overline{v}\frac{\partial \overline{T}}{\partial y} = \alpha\left[1 + \frac{16\sigma * \overline{T}_\infty^{\,3}}{3k\,k^*}\right]\frac{\partial^2 \overline{T}}{\partial y^2} + \frac{\upsilon}{C_p}\left(\frac{\partial \overline{u}}{\partial y}\right)^2 - \frac{Q_0}{\rho C_p}(\overline{T} - \overline{T}_\infty) + \frac{\sigma}{\rho C_p}B_0{}^2\overline{u}^2. \tag{8}$$

Numerical solution

In order to determine the numerical solution of the aforementioned problem the following similarity transforms [37] were introduced:

$$\eta = y(a/\upsilon)^{1/2},\ \psi(x,y) = x(a\upsilon)^{1/2} f(\eta),\ \theta(\eta) = \frac{\overline{T} - \overline{T}_\infty}{\overline{T}_w - \overline{T}_\infty} \text{ and } \phi(\eta) = \frac{\overline{\beta} - \overline{\beta}_\infty}{\overline{\beta}_w - \overline{\beta}_\infty}, \tag{9}$$

where ψ is steam function expressed as: $\overline{u} = \frac{\partial \psi}{\partial y}$ and $\overline{v} = -\frac{\partial \psi}{\partial x}$. (10)

Using Eq. (9) in (10), we obtain: $\overline{u}/xa = f'(\eta)$ and $(a\upsilon)^{-1/2}\overline{v} = -f(\eta)$, (11)

here primes indicate the differentiation with respect to η.

Eqs. (9) and (11) transform Eqs. (2), (8) and (4) in the form of three ordinary differential equations given as:

$$f'''(\eta) + f(\eta)f''(\eta) - \mathrm{M}f'(\eta) - f'(\eta)^2 = 0, \tag{12}$$

$$\frac{1}{\mathrm{Pr}}\left[\frac{3+4R}{3}\right]\theta''(\eta) - Q\theta(\eta) + f(\eta)\theta'(\eta) + \mathrm{Ec}\left[\{f''(\eta)\}^2 + \mathrm{M}f'(\eta)^2\right] = 0, \tag{13}$$

$$\phi''(\eta) + \mathrm{Sc}\,f(\eta)\phi'(\eta) - \mathrm{ScK}\phi(\eta) = 0, \tag{14}$$

subject to the associated conditions:

$$\left.\begin{aligned} &f = \mathrm{S},\ f' = \lambda,\ \theta = 1 \text{ and } \phi = 1 \text{ when } \eta = 0,\\ &f' \to 0,\ \theta \to 0 \text{ and } \phi \to 0 \text{ for } \eta \to \infty. \end{aligned}\right\} \tag{15}$$

where

$$\left.\begin{aligned} &\mathrm{Pr} = \frac{\upsilon}{\alpha}, R = \frac{4\sigma^* T_\infty'^3}{k\,k^*},\ Q = \frac{Q_0}{a\,\rho C_p},\ \mathrm{Ec} = \frac{\overline{u}_w^2}{C_p(T_w' - T_\infty')},\\ &\mathrm{M} = \frac{\sigma B_0{}^2}{a\rho},\ \mathrm{Sc} = \frac{\upsilon}{D_B},\ \mathrm{K} = \frac{k_0}{a} \text{ and } \mathrm{S} = -\frac{v_0}{\sqrt{a\upsilon}}. \end{aligned}\right\} \tag{16}$$

It may be noted that the positive and negative values of S correspond to suction and injection, respectively, whereas Q<0 signifies the sink and Q<0 indicates the source.

Skin friction, local Nusselt and local Sherwood numbers

From engineering aspects, skin friction coefficient S_f, local Nusselt number Nu_x and local Sherwood number Sh_x are, respectively, given by:

$$S_f = \tau_w\left(\rho\overline{u}_w^2(x)\right)^{-1},\ Nu_x = \left(k(\overline{T}_w - \overline{T}_\infty)\right)^{-1} x\,q_w \text{ and } Sh_x = \left(\mathrm{D}_B(\overline{\beta}_w - \overline{\beta}_\infty)\right)^{-1} x\,q_m, \tag{17}$$

where $\tau_w = \mu(\partial\overline{u}/\partial y)_{y=0}$ is used for wall shear stress, $q_w = (q_r)_{y=0} - (\partial\overline{T}/\partial y)_{y=0}$ indicates the wall heat flux and $q_m = -D_B(\partial\overline{\beta}/\partial y)_{y=0}$ signifies the wall shear mass flux. The dimensionless forms of S_f, Nu_x and Sh_x are represented as:

$$S_f = f''(0)/\mathrm{Re}_x^{1/2},\ Nu_x = -\left\{(3+4R)/3\mathrm{Re}_x^{1/2}\right\}\theta'(0) \text{ and } Sh_x = -\phi'(0)/\mathrm{Re}_x^{1/2}, \tag{18}$$

where $\mathrm{Re}_x = x\overline{u}_w/\upsilon$ represents the local Reynolds number.

Flow stability analysis

To analyze the physically reliable and stable solutions, flow stability analysis was done corresponding to the solutions of Eqs. (1) to (5) by considering their unsteady forms. The continuity Eq. (1) remains unchanged while Eqs. (2) to (4) are replaced by:

$$\frac{\partial \overline{u}}{\partial t}+\overline{u}\frac{\partial \overline{u}}{\partial x}+\overline{v}\frac{\partial \overline{v}}{\partial y}=\upsilon\frac{\partial^2 \overline{u}}{\partial y^2}-\frac{\sigma {B_0}^2}{\rho}\overline{u}, \tag{19}$$

$$\frac{\partial \overline{T}}{\partial t}+\overline{u}\frac{\partial \overline{T}}{\partial x}+\overline{v}\frac{\partial \overline{T}}{\partial y}=\alpha\frac{\partial^2 \overline{T}}{\partial y^2}+\frac{\upsilon}{C_p}\left(\frac{\partial \overline{u}}{\partial y}\right)^2-\frac{1}{\rho C_p}\frac{\partial q_r}{\partial y}-\frac{Q_0}{\rho C_p}(\overline{T}-\overline{T}_\infty)+\frac{\sigma}{\rho C_p}{B_0}^2\overline{u}^2, \tag{20}$$

$$\frac{\partial \overline{\beta}}{\partial t}+\overline{u}\frac{\partial \overline{\beta}}{\partial x}+\overline{v}\frac{\partial \overline{\beta}}{\partial y}=D_B\frac{\partial^2 \overline{\beta}}{\partial y^2}-k_0(\overline{\beta}-\overline{\beta}_\infty), \tag{21}$$

where t represents the time.

For the above unsteady problem, new similarity transforms were introduced:

$$\left.\begin{aligned}&\eta=y\sqrt{\frac{a}{\upsilon}},\ \ v=-(a\upsilon)^{1/2}f(\eta,\tau), u=a\,x\,\partial f(\eta,\tau)/\partial\eta,\\&\theta(\eta,\tau)=\left(\overline{T}_w-\overline{T}_\infty\right)^{-1}\left(\overline{T}-\overline{T}_\infty\right),\ \ \phi(\eta,\tau)=\left(\overline{\beta}-\overline{\beta}_\infty\right)\left(\overline{\beta}_w-\overline{\beta}_\infty\right)^{-1},\ \ \tau=at.\end{aligned}\right\} \tag{22}$$

Now, the Eqs. (19), (20) and (21) reduce to:

$$\frac{\partial^3 f}{\partial\eta^3}+f\frac{\partial^2 f}{\partial\eta^2}-\left(\frac{\partial f}{\partial\eta}\right)^2-\mathrm{M}\frac{\partial f}{\partial\eta}-\frac{\partial^2 f}{\partial\eta\,\partial\tau}=0, \tag{23}$$

$$\frac{1}{\mathrm{Pr}}\left[\frac{3+4R}{3}\right]\frac{\partial^2\theta}{\partial\eta^2}+f\frac{\partial\theta}{\partial\eta}-Q\theta+\mathrm{Ec}\left[\left(\frac{\partial^2 f}{\partial\eta^2}\right)^2+\mathrm{M}\left(\frac{\partial f}{\partial\eta}\right)^2\right]-\frac{\partial\theta}{\partial\tau}=0, \tag{24}$$

$$\frac{\partial^2\phi}{\partial\eta^2}+\mathrm{Sc}\,f\frac{\partial\phi}{\partial\eta}-\mathrm{Sc}\,\mathrm{K}\phi-\mathrm{Sc}\frac{\partial\phi}{\partial\tau}=0, \tag{25}$$

and the boundary conditions are converted to:

$$\left.\begin{aligned}&\partial f(\eta,\tau)/\partial\eta=\lambda,\ f(\eta,\tau)=\mathrm{S},\ \theta(\eta,\tau)=1,\ \phi(\eta,\tau)=1 \text{ when } \eta=0,\\&\partial f(\eta,\tau)/\partial\eta\to 0,\ \ \phi(\eta,\tau)\to 0,\ \ \theta(\eta,\tau)\to 0, \qquad \text{for } \eta\to\infty.\end{aligned}\right\} \tag{26}$$

To analyze the stability of the solution for the case of a steady flow $\theta(\eta)=\theta_0(\eta)$, $\phi_0(\eta)=\phi(\eta)$ and $f(\eta)=f_0(\eta)$ satisfying the problem mentioned above, the following expressions were considered [39, 40]:

$$\left.\begin{aligned}f(\eta,\tau)&=f_0(\eta)+\mathrm{e}^{-\xi\tau}X(\eta,\tau),\\\theta(\eta,\tau)&=\theta_0(\eta)+\mathrm{e}^{-\xi\tau}Y(\eta,\tau),\\\phi(\eta,\tau)&=\phi_0(\eta)+\mathrm{e}^{-\xi\tau}Z(\eta,\tau),\end{aligned}\right\} \tag{27}$$

where ξ is an unknown eigenvalue, and the functions $X(\eta,\tau), Y(\eta,\tau)$ and $Z(\eta,\tau)$ are relatively very small as compared to the functions $f_0(\eta)$, $\theta_0(\eta)$ and $\phi_0(\eta)$. The solutions of the above Eqs. (23) to (26) provide a set of an infinite number of eigenvalues $\xi_1<\xi_2<\xi_3<\ldots$. The initial growth of disturbance is found for a negative value of ξ_1 and the fluid flow becomes unstable whereas initial decay is observed for the positive value of ξ_1 and as a result the flow becomes stable. By making use of (27) in Eqs. (23) to (25), the following linearized equations were obtained:

$$\frac{\partial^3 X}{\partial\eta^3}+f_0\frac{\partial^2 X}{\partial\eta^2}+X\frac{\partial^2 f_0}{\partial\eta^2}-\left(2\frac{\partial f_0}{\partial\eta}+\mathrm{M}-\xi\right)\frac{\partial X}{\partial\eta}-\frac{\partial^2 X}{\partial\eta\partial\tau}=0, \tag{28}$$

$$\frac{1}{\mathrm{Pr}}\left[1+\frac{4R}{3}\right]\frac{\partial^2 Y}{\partial\eta^2}+f_0\frac{\partial Y}{\partial\eta}+X\frac{\partial\theta_0}{\partial\eta}+2\mathrm{Ec}\left(\frac{\partial^2 f_0}{\partial\eta^2}\frac{\partial^2 X}{\partial\eta^2}+M\frac{\partial f_0}{\partial\eta}\frac{\partial X}{\partial\eta}\right)-(Q-\xi)Y-\frac{\partial Y}{\partial\tau}=0, \tag{29}$$

$$\frac{\partial^2 Z}{\partial\eta^2}+\mathrm{Sc}f_0\frac{\partial Z}{\partial\eta}+\mathrm{Sc}X\frac{\partial\varphi_0}{\partial\eta}-(K-\xi)\mathrm{Sc}Z-\mathrm{Sc}\frac{\partial Z}{\partial\tau}=0\cdot \tag{30}$$

The associated boundary conditions are:

$$\left.\begin{aligned}&\frac{\partial X(\eta,\tau)}{\partial\eta}=0,\ X(\eta,\tau)=0,\ Z(\eta,\tau)=0,\ Y(\eta,\tau)=0,\quad \text{at } \eta=0,\\&\frac{\partial X(\eta,\tau)}{\partial\eta}\to 0,\ Z(\eta,\tau)\to 0,\ Y(\eta,\tau)\to 0,\qquad \text{as } \eta\to\infty.\end{aligned}\right\} \tag{31}$$

By putting $\tau=0$, the solutions $f(\eta)=f_0(\eta),\ \theta(\eta)=\theta_0(\eta)$ and $\phi(\eta)=\phi_0(\eta)$ of the above mentioned problem were obtained. Here, $X(\eta)=X_0(\eta),\ Y(\eta)=Y_0(\eta)$ and $Z(\eta)=Z_0(\eta)$ in Eqs. (28) to (31) classify the initial growth or decay of solution. For this, the below mentioned eigenvalue problem is required to be solved:

$$X_0'''+f_0X_0''+X_0f_0''-\left(2f_0'+\mathrm{M}-\xi\right)X_0'=0, \tag{32}$$

$$\frac{1}{\mathrm{Pr}}\left[1+\frac{4R}{3}\right]Y_0''+f_0Y_0'+X_0\theta_0'+2\mathrm{Ec}\left(f_0''X_0''+\mathrm{M}f_0'X_0'\right)-\left(Q-\xi\right)Y_0=0, \tag{33}$$

$$Z_0''+\mathrm{Sc}f_0Z_0'+X_0\varphi_0'-\left(\mathrm{K}-\xi\right)\mathrm{Sc}Z_0=0, \tag{34}$$

together with the associated boundary conditions:

$$\left.\begin{aligned}&X_0'(0)=0,\ Y_0(0)=0,\ X_0(0)=0,Z_0(0)=0,\\&Y_0(\eta)\to 0,X_0'(\eta)\to 0,\ \ Y_0(\eta)\to 0\ \text{as}\ \eta\to\infty.\end{aligned}\right\} \tag{35}$$

It is observed that the stability of solution $f_0(\eta),\ \theta_0(\eta)$ and $\phi_0(\eta)$ corresponding to the steady flow can be analyzed by the least eigenvalue ξ for the pertinent flow parameters. Moreover, the possible eigenvalues range can be evaluated by relaxing the boundary condition on $X_0'(\eta), Y_0(\eta)$ and $Z_0(\eta)$ as mentioned by Harris *et al*. [41]. In this problem, the condition $X_0'(\eta)\to 0$ as $\eta\to\infty$ has been relaxed and we imposed a new boundary condition $X_0''(\eta)=1$ in order to obtain the solution of Eqs. (32) to (34).

Analytical solution

The exact solution of Eq. (12) satisfying the conditions (15) can be determined as shown below:

$$f_0(\eta)=\mathrm{S}+\frac{\lambda\left(1-e^{-\delta\eta}\right)}{\delta}, \tag{36}$$

where

$$\delta=\frac{\mathrm{S}\pm\sqrt{\mathrm{S}^2+4(\lambda+\mathrm{M})}}{2}. \tag{37}$$

From Eqs. (36) and (37) it may be noted that dual solutions exist for $f_0(\eta)$ provided $S^2+4(\lambda+M) > 0$, one real solution occurs if $S^2+4(\lambda+M) = 0$ and the problem has no real solution whenever $S^2+4(\lambda+M) < 0$. The critical value λc at which no real solution occurs can be easily determined as:

$$\lambda_c=-\frac{\left(\mathrm{S}^2+4\mathrm{M}\right)}{4}<0. \tag{38}$$

From the above exact analysis, the value of wall velocity gradient was obtained as:

$$f_0''(0)=-\delta\lambda. \tag{39}$$

NUMERICAL METHOD IMPLEMENTATIONS

To obtain the solutions of the mentioned governing equations the 4th order Runge-Kutta scheme along with a shooting technique was employed. Foremost, the prevailing equations were converted using the suitable similarity variables into a set of five differential equations of first order. Then, the Runge-Kutta method of 4th order was applied to solve the resulting equations, wherein the initial guess for $f''(0), \theta'(0)$ and $\phi'(0)$ was analyzed employing a shooting technique. The initial guess was corrected by means of the Secant method. Throughout the study, the tolerance error was considered as 10^{-6} to gain more precise results.

RESULTS AND DISCUSSION

The numerical computation was executed and the results were reported to demonstrate a comparative study showing the impacts of various parameters such as S (suction/injection), M (magnetic field), λ (stretching/shrinking), Ec (Eckert number), R (thermal radiation), Q (heat absorption), Pr (Prandtl number), Sc (Schmidt number) and K (chemical reaction) on the flow field. Figs. 2-16 represent the profiles of fluid velocity, temperature distribution and concentration for the varying relevant flow parameters which portray that the boundary layer thickness in the case of a lower branch solution is wider compared to that of an upper branch solution. Further, the existence of profiles of two types was noticed for a specific value of the flow parameter which supports the dual solutions existence. Also, these profiles satisfy the outlying boundary conditions mentioned in (15) asymptotically which validates the computational results of the solution. Figs. 2 to 7 demonstrate that due to the rise of suction and magnetic parameters, i.e. S and M, the fluid velocity $|f'(\eta)|$ and fluid temperature $\theta(\eta)$ get decreased in the regime of boundary layer for an upper branch solution. $|f'(\eta)|$and $\theta(\eta)$ get increased in case of a lower branch solution while the shrinking parameter $\lambda(<0)$ increases $|f'(\eta)|$ and $\theta(\eta)$ in case of an upper branch solution and reduces in a lower branch solution. Enhancement of fluid temperature was observed in the cases of both upper and lower branch solutions due to the augmenting values of R and Ec as is depicted in Figs. 8 and 9. Physically Ec represents the ratio of kinetic energy and enthalpy, which converts the kinetic energy to the form of internal energy in opposition to viscous fluid stresses. For that reason, the viscous dissipation tends to enhance fluid temperature. Figs. 10 and 11 depict that for both upper and lower branch solutions the fluid temperature $\theta(\eta)$ diminishes due to the rising values of Q and Pr which implies that heat absorption has impeding impact on fluid temperature while thermal diffusion has overturn impact on it in the regime of flow. The variations in species concentration $\phi(\eta)$ for varying M, S, λ, Sc and K are presented in Figs. 12 to 16. In these figures, dual concentration profiles $\phi(\eta)$ depict that rising values of M and S result in a net reduction in $\phi(\eta)$ in case of an upper branch solution and augment in a lower branch solution whereas the shrinking parameter $\lambda(<0)$ has a reverse impact on it. But for both branches of solutions, $\phi(\eta)$ decreases on increasing the values of Sc and K, which demonstrates that the chemical reaction reduces the fluid concentration while mass diffusion has a reverse impact on it. Moreover, the wall velocity gradient *f"(0)* profiles displayed in Figs. 17 and 18 quantify the impacts of suction parameter S (>0) and magnetic parameter M taking into consideration the shrinking sheet $(\lambda<0)$.

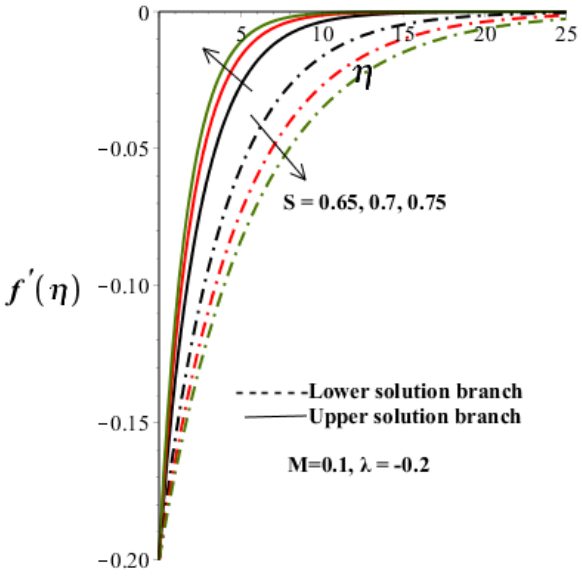

Fig. 2. Velocity profiles with increasing S.

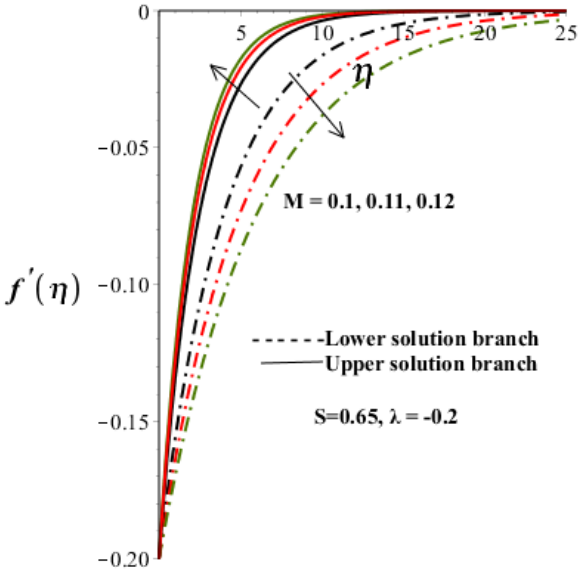

Fig. 3. Velocity profiles with increasing M.

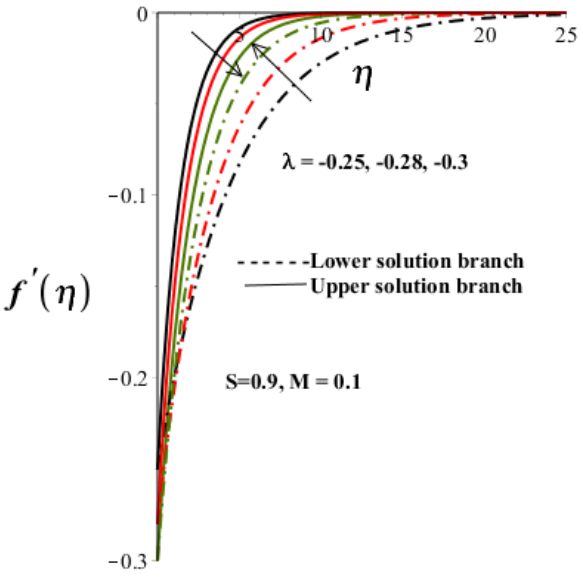

Fig. 4. Velocity profiles with increasing shrinking parameter λ<0.

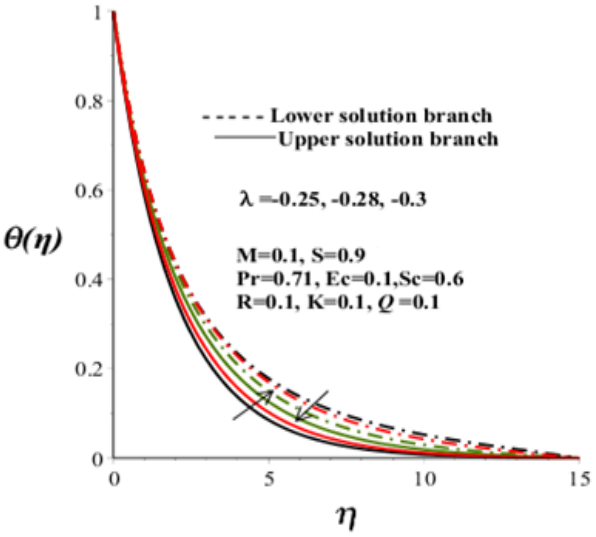

Fig. 7. Temperature profiles with increasing shrinking parameter λ<0.

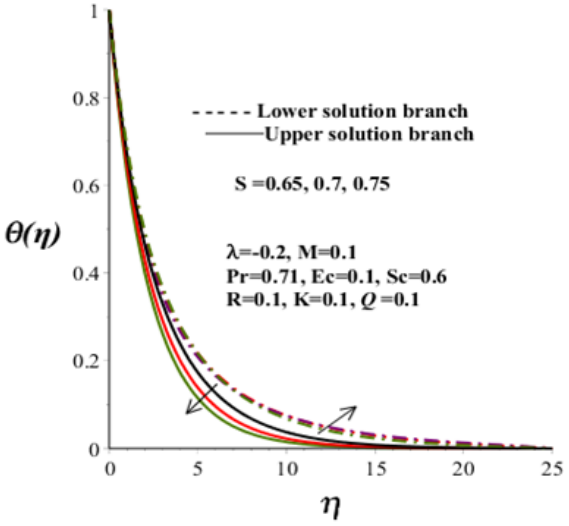

Fig. 5. Temperature profiles with increasing S.

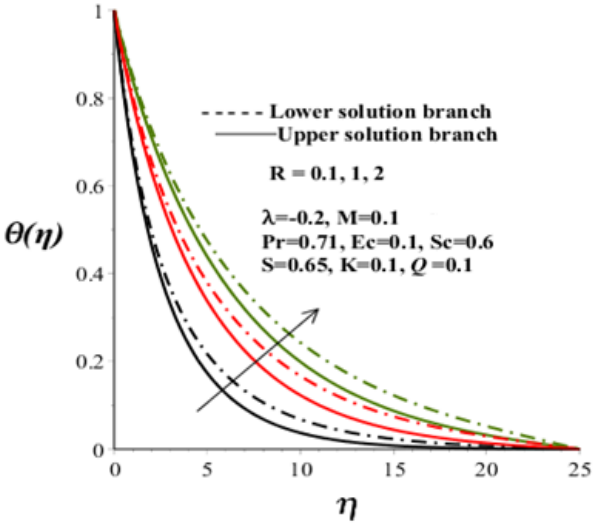

Fig. 8. Temperature profiles with increasing R.

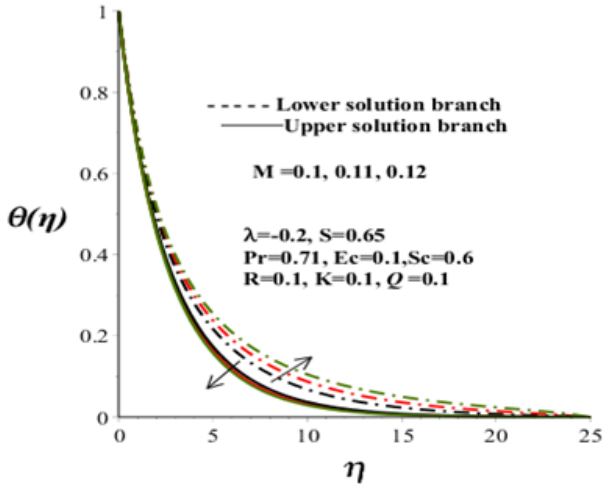

Fig. 6. Temperature profiles with increasing M.

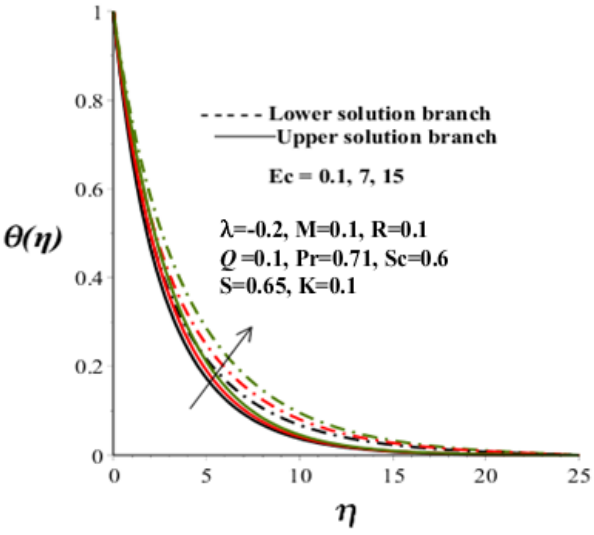

Fig. 9. Temperature profiles with increasing Ec.

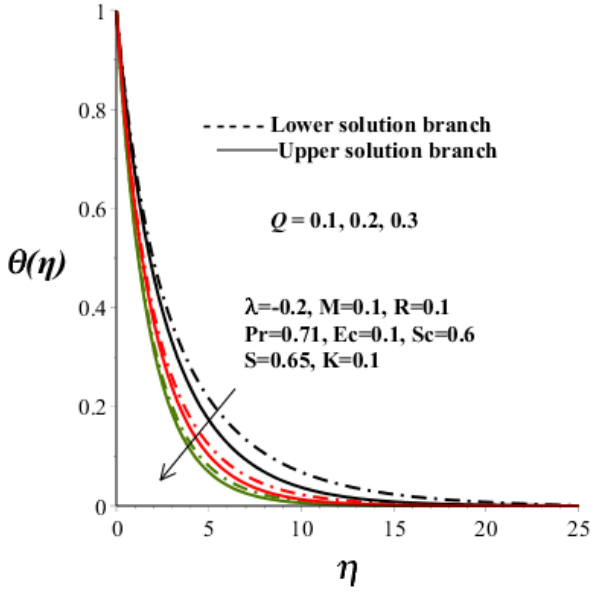

Fig. 10. Temperature profiles with increasing Q.

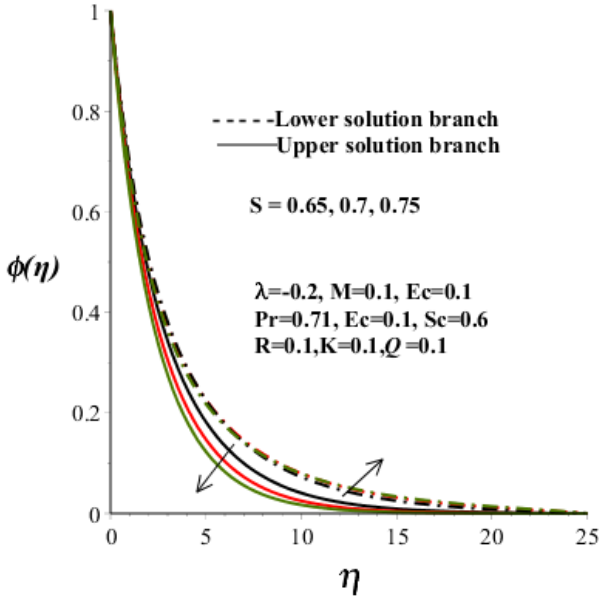

Fig. 13 Concentration profiles with increasing *S*.

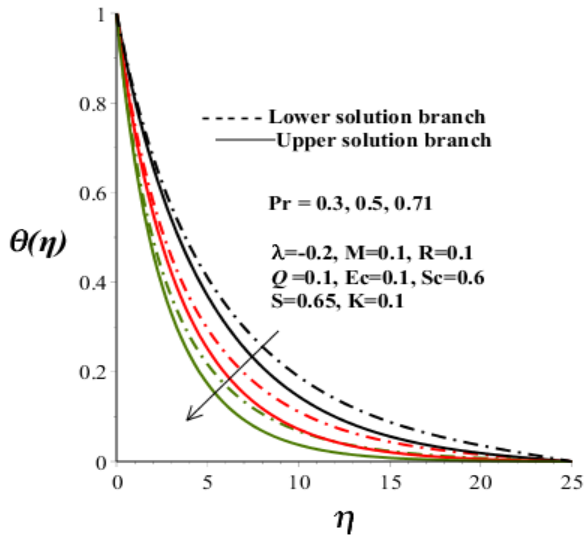

Fig. 11. Temperature profiles with increasing *Pr*.

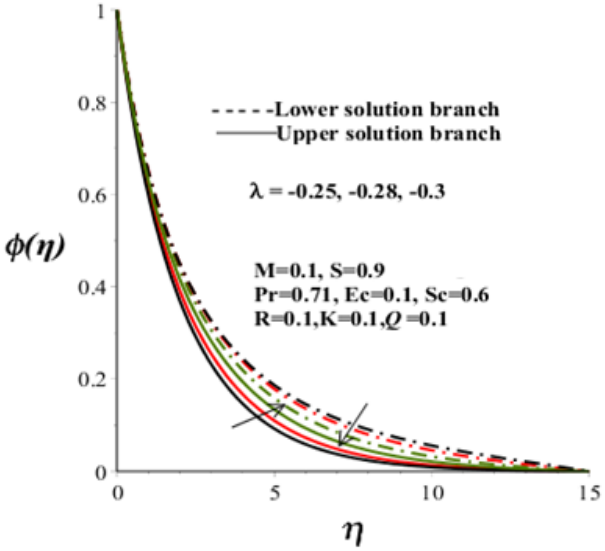

Fig. 14. Concentration profiles with increasing shrinking parameter $\lambda<0$.

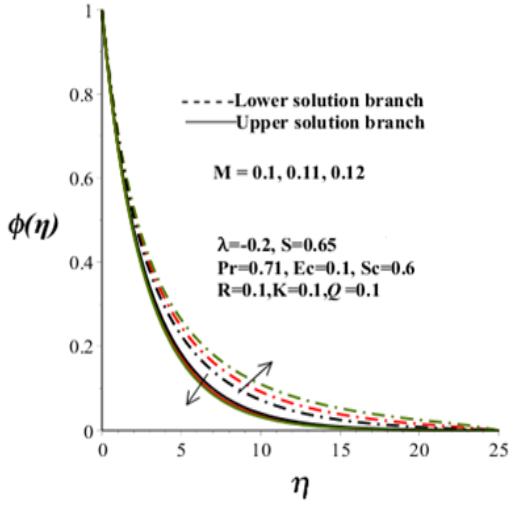

Fig. 12. Concentration profiles with increasing *M*.

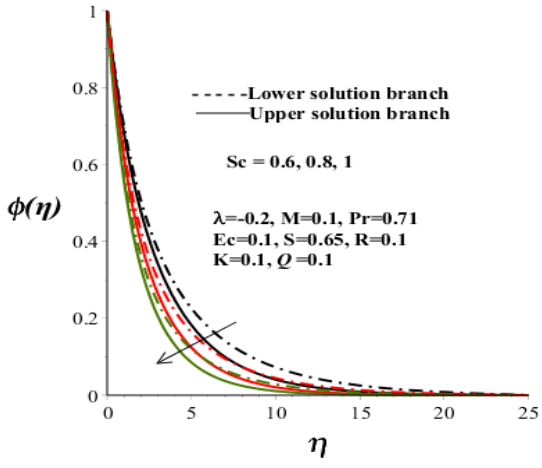

Fig. 15. Concentration profiles with increasing Sc.

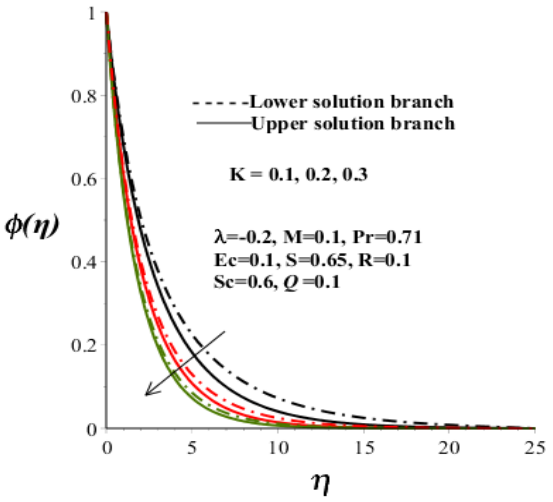

Fig. 16. Concentration profiles with increasing *K*.

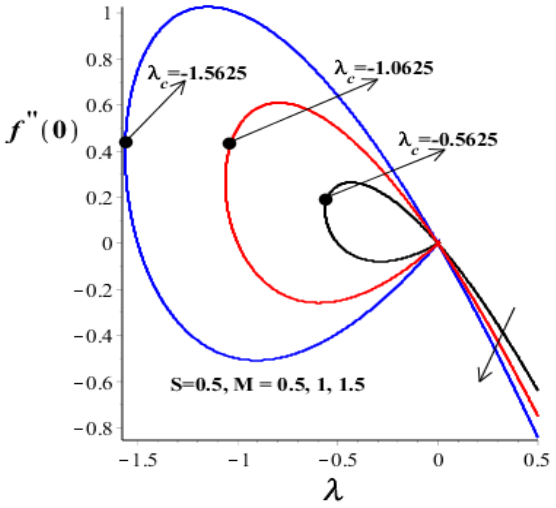

Fig. 18. Variation of $f''(0)$ with increasing M and λ.

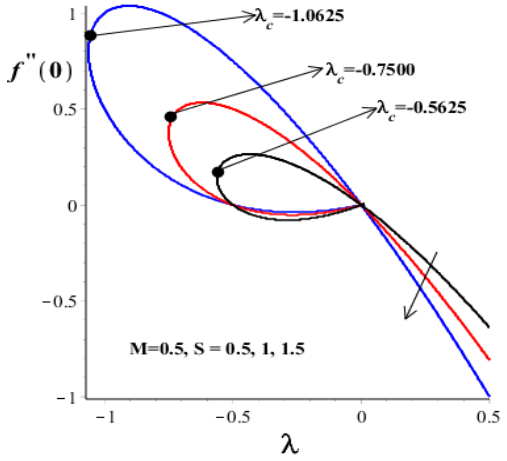

Fig. 17. Variation of $f''(0)$ with increasing S and λ.

Table 1. Computations showing the critical values of the shrinking parameter λ_c for different values of M and S.

M	S	λ_c
0.5	0.1	-0.5025
0.5	0.5	-0.5625
0.5	1	-0.7500
0.5	2	-1.5000
1	0.1	-1.0025
1	0.5	-1.0625
1	1	-1.2500
1	2	-2.0000

Table 2. Computations showing the smallest eigenvalues ξ_1 at various values of the shrinking sheet parameter (λ<0)

M	S	λ	ξ_1 (Upper branch)	ξ_1 (Lower branch)
0.7	1	-0.4	0.8738795538	-0.442442016
0.7	1	-0.5	0.8168841346	-0.485765277
0.7	1	-0.6	0.7468719153	-0.500942232
0.7	1.2	-0.4	0.9804155402	-0.444083502
0.7	1.2	-0.5	0.9266000714	-0.500599337
0.7	1.2	-0.6	0.8647294919	-0.533302779
0.72	1	-0.4	0.8962607582	-0.448818328
0.72	1	-0.5	0.8406711179	-0.494098385
0.72	1	-0.6	0.7729698714	-0.512498179
0.72	1.2	-0.4	1.0022753340	-0.448862076
0.72	1.2	-0.5	0.9494123019	-0.507306837
0.72	1.2	-0.6	0.8889867027	-0.542405698

These figures reveal the existence of a unique solution of the reported problem when $\lambda > 0$, dual (lower and upper branch) solutions when $\lambda_c < \lambda \leq 0$ and no solution for the case of $\lambda < \lambda_c$, where $\lambda_c < 0$ represents the critical value of the shrinking parameter λ beyond which no solution of the problem exists. In addition to it, the wall velocity gradient $f''(0)$ gets increased in magnitude for rising values of S and M which shows that the shear stress gets augmented at the shrinking sheet due to suction and magnetic field. The critical values of the shrinking parameter λ_c for varying values of M and S are provided in Table 1.

In order to determine the physically reliable and stable solutions, the reported eigenvalue problem was solved to obtain the smallest eigenvalue ξ_1. The initial growth of disturbance was found for negative values of ξ_1 and the fluid flow becomes unstable whereas initial decay is observed for positive values of ξ_1 and as a result the flow becomes stable. The computations showing the smallest eigenvalue ξ_1 at numerous values of the shrinking sheet parameter $(\lambda < 0)$ are shown in Table 2. The computational results of the table indicate that ξ_1 is positive for the upper branch solution whereas it is negative in the case of lower branch solution. Hence, the upper branch solution is physically reliable and stable whilst the lower branch solution is not.

From an engineering aspect, the numerical values of S_f, Nu_x and Sh_x are obtained for the different flow parameters, which are presented in Tables 3 to 5. These tables reveal that the wall velocity gradient $f''(0)$ gets increased in magnitude for increasing values of M, λ and S while the wall temperature gradient $\theta'(0)$ decreases in magnitude with the increase in either M or λ or R or Ec and it increases on increasing either S or Q or Pr. Physically it is construed that a shear stress at the stretched sheet gets augmented due to intensification of suction, magnetic field, and velocity slip factor whereas heat transfer rate at the stretched sheet gets reduced due to velocity slip factor, magnetic field, thermal radiation, viscous and thermal diffusions where there is a reverse impact of suction and heat absorption. The mass transfer rate at the surface of a stretched sheet is enhanced due to the chemical reaction whereas it gets reduced due to the mass diffusion.

Table 3. Numerical values of the velocity wall gradient.

M	λ	S	$-f''(0)$
0.05			4.416576
0.2			4.467439
0.6			4.598301
	-1.1		3.722558
	-1.3		4.467439
	-1.5		5.231191
		2.5	3.899999
		3.0	4.467439
		3.5	5.051801

VALIDATION OF THE NUMERICAL ALGORITHM

To justify the numerical algorithm used in the present study, we have presented a comparison of Nusselt number in the limiting sense with those of Yasin *et al*. [37]. This comparison portrays an excellent agreement of our results, as is evident from Table 6. This validates the implemented numerical algorithm of the present study along with the correctness of the obtained results.

Table 4. Numerical values of the temperature wall gradient.

M	λ	S	R	Ec	Q	Pr	$-\theta'(0)$
0.05							2.044389
0.2							2.043783
0.6							2.042221
	-1.5						2.062335
	-1.3						2.043783
	-1.1						2.024837
		2.5					1.753439
		3.0					2.043783
		3.5					2.338760
			0.1				2.043783
			0.3				1.668829
			0.5				1.412152
				0.1			2.043783
				0.3			2.018168
				0.5			1.992553
					0.1		2.043783
					1.1		2.301413
					2.1		2.516904
						0.3	0.896613
						0.5	1.460278
						0.71	2.043783

Table 5. Numerical values of the concentration wall gradient.

Sc	K	$-\phi'(0)$
0.6		2.081344
0.8		2.711802
1.0		3.336434
	0.25	3.266926
	0.5	3.336434
	0.75	3.403398

Table 6. Numerical values of Nusselt number when $M = 0.2,\ \lambda = -1.3,\ S = 3, Q = 0.1,\ \mathrm{Pr} = 0.71$ and $\mathrm{Ec} = 0$

R	Present work	Yasin *et al*. [37]
0	-2.319237	-2.31923
0.1	-2.056590	-2.05659
0.5	-1.420937	-1.42093

CONCLUSIONS

The numerical computations of a two-dimensional steady MHD heat and mass transfer boundary layer flow of an incompressible, optically thick radiative, heat absorbing, electrically conducting viscous fluid driven by a stretched/shrinking sheet in the presence of a homogeneous chemical reaction were performed to quantify the impacts of relevant flow parameters. The results revealed the existence of dual solutions. For the stretching sheet a unique solution was found whilst a dual solution was accounted for the shrinking sheet. The stability analysis conferred that an upper branch solution is physically reliable and stable whereas a lower branch solution is not. The stretching/shrinking parameter range is widened due to suction and magnetic field for which the solution exists. For a physically reliable solution, the shear stress at a stretched/shrinking sheet gets augmented owing to suction and magnetic field.

Conflict of interest: *There is no conflict of interest of authors with any researcher doing research in this area.*

REFERENCES

1. K. B. Pavlov, *Magnetohydrodynamics*, **10,** 507 (1974).
2. A. Chakrabarti, A. S. Gupta, *Quart. Appl. Math*., **37,** 73 (1979).
3. M. Q. Al-Odat, R. A. Damseh, T A Al-Azab, *Int. J. Appl. Mech. Eng*., **11,** 289 (2006).
4. A. Ishak, R. Nazar, I. Pop, *Nonlinear Anal.: Real World Applications*, **10,** 2909 (2009).
5. O. D. Makinde, W. A. Khan, Z. H. Khan, *Int. J. Heat Mass Transfer*, **62,** 526 (2013).
6. T. Hayat, S. A. Shehzad, A. Alsaedi, *J. Aerospace Eng*., **27,** 1 (2014).
7. Y. Khan, *Sci. Iran. B*, **24,** 2466 (2017).
8. E. M. A. Elbashbeshy, *Arch. Mech*., **53,** 643 (2001).
9. E. M. A. Elbashbeshy, M. A. A. Bazid, *Appl. Math. Comp*., **138,** 239 (2003).
10. E. M. A. Eldahab, M. A. E. Aziz, *Int. J. Thermal Sci*., **43,** 709 (2004).
11. O. D. Makinde, W. A. Khan, J. R. Culham, *Int. J. Heat Mass Transfer*, **93,** 595 (2016).
12. O. D. Makinde, F. Mabood, W. A. Khan, M. S. Tshehla, *J. Molecular Liquids*, **219,** 624 (2016).
13. O. D. Makinde, K. G. Kumar, S. Manjunatha, B. J. Gireesha, *Defect Diff. Forum*, **378,** 125 (2017).
14. O. D. Makinde, I. L. Animasaun, *Int. J. Ther. Sci.,* **109,** 159 (2016).
15. O. D. Makinde, *Z. Naturforsch.*, **67,** 239 (2012).
16. O. D. Makinde, *Meccanica*, **47,** 1173 (2012).
17. N. Ali, S. U. Khan, Z. Abbas, M. Sazid, *J. Braz. Soc. Mech. Sci. & Eng.*, **38,** 2533 (2017).
18. K. Vajravelu, A. Hadjinicolaou, *Int. Comm. Heat Mass Transfer*, **20,** 417 (1993).
19. M. K. Partha, P. V. S. N. Murthy, G. P. Rajasekhar, *Heat Mass Transfer*, **41,** 360 (2005).
20. R. Cortell, *Phys. Letters A*, **372,** 631 (2008).
21. E. M. A. Aziz, *Canadian J. Phys.*, **87,** 359 (2009).
22. D. S. P. Anjali, B. Ganga, *Nonlinear Anal: Mod. Control*, **14,** 303 (2009).
23. D. Pal, *Appl. Math. Comp.*, **217,** 2356 (2010).
24. G. S. Seth, J. K. Singh, *Appl. Math. Mod*., **40,** 2783 (2016).
25. G. S. Seth, S. Sarkar, O. D. Makinde, *J. Mech*., **32,** 613 (2016).
26. G. S. Seth, R. Sharma, M. K. Mishra, A. J. Chamkha, *Eng. Comp*., **34,** 603 (2017).
27. G. S. Seth, R. Tripathi, M. K. Mishra, *Appl. Math. Mech. –Eng. Ed.*, **38,** 1613 (2017).
28. J. Zueco, S. Ahmed, *Appl. Math. Mech. –Eng. Ed.*, **31,** 1217 (2010).
29. R. Nandkeoylyar, M. Das, P. Sibanda, *Math. Prob. Eng*., **2013,** 1 (2013).
30. A. O. Ajibade, A. M. Umar, *Int. J. Energy Tech.*, **6,** 1 (2014).
31. M. M. Rashidi, E. Momoniat, M. Ferdows, A. Basiriparsa, *Math. Prob. Eng*., **2014,** 1 (2014).
32. M. Ganapathirao, R. Ravindran, E. Momoniat, *Heat Mass Transfer*, **51,** 289 (2015).
33. M. Sheikh, Z. Abbas, *J. Magn. Magn. Mater.*, **396,** 204 (2015).
34. N. Freidoonimehr, M. M. Rashidi, B. Jalilpour, *J. Braz. Soc. Mech. Sci. & Eng.*, **38,** 1999 (2016).
35. S. M. Hussain, J. Jain, G. S. Seth, *Bul. Chem. Comm.*, **48,** 659 (2016).
36. S. M. Hussain, J. Jain, G. S. Seth, M. M. Rashidi, *J. Magn. Magn. Mater.*, **422,** 112 (2017).
37. M. H. Yasin, A. Ishak, I. Pop, *J. Magn. Magn. Mater*., **407,** 235 (2016).
38. A. Raptis, *Thermal Sci*., **15,** 849 (2011).
39. P. D. Weidman, A. M. J. Davis, *Int. J. Eng. Sci*., **44,** 730 (2006).
40. A. Postelnicu, I. Pop, *Appl. Math. Comp.*, **217,** 4359 (2011).
41. S. D. Harris, D. B. Ingham, I. Pop, *Trans. Porous Media*, **77,** 267 (2009).